Nanoscale

Accepted Manuscript

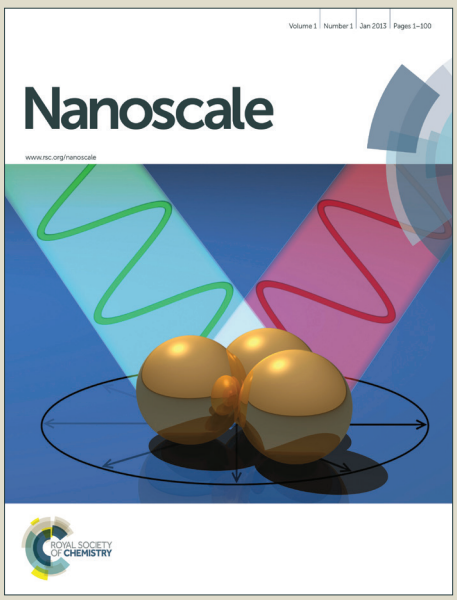

ROYAL SOCIETY OF CHEMISTRY

www.rsc.org/nanoscale

Manipulating the charge transfer at CuPc/graphene interface by O_2 plasma treatments

Hongying Mao*[a], Fang Hu[b,c], Quan-Lin Ye[a], Yifeng Xu[a], Xuxin Yang[a], Bin Lu*[d]

[a] Department of Physics, Hangzhou Normal University, Hangzhou 310036, China

[b] Ningbo Institute of Technology, Zhejiang University, Ningbo 315100, China

[c] Department of Physics, Zhejiang University, Hangzhou 310027, China

[d] State Key Laboratory of Silicon Materials, Department of Materials Science and Engineering, Zhejiang University, Hangzhou 310027, China

The manipulation of charge transfer at CuPc/graphene interface has been demonstrated by treating the pristine graphene with O_2 plasma. As revealed by *in situ* ultraviolet photoelectron spectroscopy measurements, a much stronger interfacial charge transfer occurs when the pristine graphene is exposed to O_2 plasma prior to the growth of CuPc films, which is attributed to the increased work function of graphene after O_2 plasma treatments. Moreover, the highest occupied molecular orbital leading edge of CuPc locates at ~ 0.80 eV below substrate Fermi level on O_2 plasma treated graphene, whereas it locates at ~ 1.10 eV on pristine graphene. Our findings provide detailed studies about the electronic structure at CuPc/graphene and CuPc/O_2 plasma treated graphene interfaces. The increased work function in combination with the relatively smaller energy offset between the highest occupied molecular orbital of CuPc and Fermi level of O_2 plasma treated graphene facilitate the extraction of holes at the interface, and hence pave the way for improving the device performance of graphene-based organic photovoltaic cells.

*Corresponding author. Email address: phymaohy@gmail.com (H. Mao) Binlu@zju.edu.cn (B. Lu)

Introduction

Due to the prospect of low cost, solution processability, and high flexibility, organic photovoltaic cells (OPVs) have been regarded as a promising solution to energy and environmental issues in a post silicon era. With great efforts in the synthesis of novel active layer, optimization of device structures, and fabricating techniques, the performance of OPVs has increased dramatically.[1-4] Recently, power conversion efficiency (PCE) of over 9% have been reported.[5, 6] However, several challenges still remain for the practical application of OPVs, including further improvement of the PCE, lowering the fabrication cost, and enhancing the cell life-time at ambient condition.[7, 8]

As a landmark transparent electrode material, indium tin oxide (ITO) has been widely used for most OPVs. However, the use of ITO is inhibited because of the diminishing supply and high cost of indium, the intrinsic brittleness, and the sensitivity to acids that is commonly used as the hole transport layer (HTL). On the other hand, there has been a growing interest in the application of graphene as a promising low cost alternative of ITO taking advantage of its high transparency, high carrier mobility, chemical robustness, and flexibility.[9-11] Many groups have already demonstrated the realization of graphene-based OPVs, but the PCE remains low compared to that of their ITO counterparts.[12-14] In order to achieve better device performance, various approaches have been developed to modify the physical and chemical properties of graphene. For example, graphene treated by O_2 plasma or UV/ozone has shown great potentials for transparent electrode applications.[15, 16]

Not only for transparent electrode materials, but also can graphene and its derivatives be used as interface layer materials. The most commonly used interface layer material is poly(3,4-ethylenedioxythiophene):poly(styrenesulfonate) (PEDOT:PSS), which helps to planarize ITO surface roughness, and facilitates the extraction of holes via an ohmic-contact at the interface between active layer and anode.[17] However, PEDOT:PSS is usually deposited from highly acidic aqueous suspensions that is detrimental to the ITO electrode. Moreover, its hygroscopic nature can introduce

water into the active layer, degrading the device performance and life-time.[18] Recently, graphene oxide (GO) and reduced graphene oxide (rGO) have been demonstrated to be a novel solution-processable alternative to PEDOT:PSS as the effective HTL in OPVs.[19-25] In the presence of oxygenated species, i.e. epoxy, hydroxyl, and carboxyl groups, the work function (WF) of GO or rGO modified anode increases to ~ 5.0 eV which matches well with the highest occupied molecular orbital (HOMO) of donor materials, and hence facilitating the extraction of holes.

For OPVs, it is well recognized that the interfacial electronic structure is of great importance in determining the device performance.[26-31] The hole injection barrier is determined by the energy offset between the HOMO of donor material and the Fermi level of anode; while the energy offset between the HOMO of donor material and the lowest unoccupied molecular orbital (LUMO) of acceptor material shows a close relationship with the open circuit voltage (V_{oc}).[32, 33] The electronic structure at the active layer/ITO interface has been well studied.[34] However, for graphene-based OPVs, there is few study about the detailed interfacial electronic structure between donor materials and graphene,[35] in particular at the interface between donor materials and oxygenated species modified graphene, such as GO, rGO, and O_2 plasma treated graphene (O_2-G). In the present study, using *in situ* ultraviolet photoelectron spectroscopy (UPS), we have demonstrated the manipulation of charge transfer at the interface between copper phthalocyanine (CuPc), a commonly used donor material, and graphene using O_2 plasma treatments. It is found that the degree of charge transfer at CuPc/O_2-G interface is much stronger than that at CuPc/graphene interface, which is attributed to the higher WF of O_2-G (~ 4.92 eV). Moreover, the oxidation degree of graphene is investigated using X-ray photoelectron spectroscopy (XPS) and Raman spectroscopy.

Experimental

Synthesis of CVD graphene

The growth of CVD graphene was carried out in a quartz tube at reduced pressure.

The copper foil (25 μm thick, 99.999% purity) was annealed at 1000°C for 30 min under a combined flow of Ar:H_2=5:1 (10 sccm) prior to the growth of graphene. Ar gas was then replaced by high purity of methane (99.999%), a gas mixture of CH_4 (30 sccm) and H_2 (10 sccm) was used for the growth of graphene. After 30 min of growth, the system was cooled down to room temperature under H_2.

Preparation of O_2-G

A parallel-plate, 13.57 MHz radio-frequency (rf) plasma system was used to prepare O_2-G samples at room temperature. The rf power was kept at 2.0 W, while the chamber pressure was kept at ~ 0.15 mbar. For contact angle goniometry and Raman measurements, CVD graphene films were transferred to SiO_2/Si substrate (300 nm thermal oxide) using normal wet-transfer technology based on poly(methyl methacrylate) (PMMA).[15] After that, graphene/SiO_2 samples were exposed to O_2 plasma for 5, 30, 120, 300, and 600 s, respectively. For UPS and XPS measurements, CVD graphene on copper foil was exposed to O_2 plasma directly.

Characterizations

In situ UPS and XPS measurements were carried out in a multifunctional ultrahigh vacuum (UHV) VT-SPM system (Omicron Instruments for Surface Science) with a base pressure better than 2×10^{-10} mbar. UPS measurements were performed with He I (21.2 eV) as the excitation source. Vacuum level shifts were measured from the linear extrapolation of the low kinetic energy part of UPS spectra with a -5 V sample bias. XPS measurements were performed with an Al Kα source (1486.6 eV). Vacuum sublimation purified CuPc molecule was thermally evaporated onto the graphene and O_2-G substrates at room temperature from a resistive-heating tantalum (Ta) boat in the growth chamber. Deposition rate, calibrated by a quartz-crystal-microbalance (QCM), of 0.3 nm/min was chosen in our UPS and XPS measurements. The binding energy of all UPS and XPS spectra were calibrated and referenced to the Fermi level of a sputtered clean gold sample. The Raman spectra were acquired using Renishaw inVia Raman Microscope (514 nm laser excitation). The focused laser spot was about 1 μm with a constant power of ~1 mW. An integration time of 10 s was used during the measurement to reduce the heating effects induced by the laser. Each Raman spectrum

shown in the present study was the average of 10 different spectra that were randomly chosen on sample surface. The contact angle measurement was carried out under ambient conditions. A 0.5 μL de-ionized water droplet has been released onto the pristine graphene and O_2-G surfaces from a syringe needle. The image of the liquid droplet was obtained in real time using a CCD camera. Contact angle data of 15 measurements per sample were averaged.

Results and discussion

To investigate the effect of O_2 plasma treatments on the electronic structure of graphene, *in situ* UPS measurements have been performed. As measured from the linear extrapolation of the low kinetic energy region in Fig. 1a, an upward shift of vacuum level of ~ 0.52 eV is observed after the pristine graphene was exposed to O_2 plasma for 600 s, or WF increases from ~ 4.40 eV to ~ 4.92 eV, indicating a p-type doping of graphene. Fig. 1b shows the UPS spectra at the low binding energy region (valence band region). Two prominent peaks for the pristine graphene on copper foil can be identified. Peak I locates at ~ 2.30 eV below substrate Fermi level, deriving from Cu 3d states of metallic copper foil,[36] and peak II locates at ~ 3.0 eV, arising from C 2p states of graphene.[37] A gradual attenuation of the intensity of peak II is observed with the increasing O_2 plasma exposure time, indicating that the native electronic structure of pristine graphene has been disrupted since some sp^2 carbon atoms have been converted into sp^3 ones after O_2 plasma treatments.

In order to evaluate the sample quality and the change of intrinsic physical property of graphene after O_2 plasma treatments, Raman measurements have been performed. Fig. 2a shows the Raman spectra of pristine graphene and O_2-G with the increasing exposure time. For pristine graphene, the Raman spectrum is dominated by the G band at ~ 1589 cm^{-1} and the second-order 2D band at ~ 2694 cm^{-1}. Its single-layer character is confirmed by the intensity ratio of 2D to G band (~ 2.9) and the FWHM (~36 cm^{-1}) of the 2D band. The disorder and defects related peak, or D band, can also be observed at ~ 1348 cm^{-1}. However, the low I_D/I_G intensity ratio of ~ 0.03 indicates the low defect density. After exposed to O_2 plasma, three significant changes can be

observed: (1) the peak intensity of D band increases with the increasing exposure time, indicating that the π conjugated structure of pristine graphene is disturbed after O_2 plasma exposure; (2) an apparently broadening of the G band, and a "shoulder" D′ band appears at the higher frequency region (~ 1620 cm^{-1}). Although both the D and D′ bands are induced by disorder or defects related features, the mechanism is different: the D band is due to intervalley, while the D′ band is due to intravalley resonant Raman scattering;[38, 39] (3) a gradual attenuation as well as the broadening of the 2D band. Moreover, since the vibrational modes of graphene are sensitive to the changes of charge carrier concentration, or Fermi level shift,[40, 41] Raman spectra have been used to confirm the p-type doping of graphene as revealed by our UPS measurements. Fig. 2b and c display the spectral shifts of graphene after O_2 plasma treatments. A blue shift of ~10 cm^{-1} and ~12 cm^{-1} can be observed for G and 2D band, respectively, which is the evidence for the p-type doping of graphene.[42, 43] The mechanism of p-type doping of graphene after O_2 plasma treatment is most likely due to the local electric dipoles on O_2-G surface in the presence of oxygenated species. Being more electronegative than carbon atoms, local electric dipoles pointing from the oxygen atom to the carbon atom are formed, which downshift the Fermi level of graphene, and hence the p-type doping. In addition to the blue shift for both G and 2D band, we also notice that there is nearly no change for the peak intensity of G band, while the peak intensity of 2D band decreases after O_2 plasma treatments. According to previous studies, the decreased relative intensity ratio between 2D and G band support the p-type doping of graphene after O_2 plasma treatments.[44]

To further study the surface properties of O_2-G, XPS measurements are exploited to quantitatively investigate the introduction of oxygenated species and their evolutions with the increasing O_2 plasma exposure time. According to previous studies,[45, 46] the C 1s spectrum of graphene and O_2-G can be fitted by four components, P1 (~ 284.4 eV), P 2 (~285.2 eV), P 3 (~286.3 eV), and P 4 (~288.2 eV), corresponding to sp^2 carbon atoms, sp^3 hybridized carbon atoms, epoxy and carbonyl groups, and carboxyl group, respectively. As shown in Fig. 3a, the C 1s spectrum is mainly dominated by the P 1 peak for pristine graphene. After exposed to O_2 plasma (Fig. 3b-d), the intensity of P 2,

P 3, and P 4 peaks increase gradually, whereas the intensity of P 1 peak decreases. By analyzing the integrated intensities of these four spectral components, it is found that only ~ 7% carbon atoms are oxidized for pristine graphene, but it increases to ~ 24% after exposed to O_2 plasma for 600 s, confirming the introduction of oxygenated species. Meanwhile, the relative intensity ratio of P 2 peak, corresponding to sp^3 hybridized carbon atoms, increases from ~ 9% to ~ 22%, suggesting the generation of fresh defective carbon domains which is consistent with the increasing peak intensity of D band in our Raman measurements. The introduction of oxygenated species after O_2 plasma treatments can also modulate the surface energy of graphene, and hence its wettability. As shown in Fig. 4, there is a drastic change in the contact angle of the water droplet with graphene before and after O_2 plasma treatments. The contact angle of pristine graphene (~ 87.6^o) exhibits its hydrophobic nature. After O_2 plasma treatments, the O_2-G surface becomes more hydrophilic with the contact angle decreasing rapidly to ~ 4.2^o. The introduction of oxygenated species after O_2 plasma treatments has also induced a significant effect on the graphene conductivity, the sheet resistance of pristine graphene and O_2-G with increasing O_2 plasma exposure time was measured by 4 point probe method, as shown in Fig. S1. The sheet resistance of graphene increased from 0.9 kΩ/sq for non-treated sample to larger than 10 MΩ after exposed to O_2 plasma for 600 s.

In order to investigate the electronic structure at CuPc/graphene and CuPc/O_2-G interfaces, *in situ* UPS measurements have been carried out. Fig. 5 shows the evolution of the thickness-dependent UPS spectra for the growth of CuPc on pristine graphene. The vacuum level shifts to lower kinetic energy part by ~ 0.30 eV with the increasing coverage of CuPc films (Fig. 5a), or the WF is gradually decreased from ~ 4.40 eV to ~ 4.10 eV after the growth of 10 nm CuPc on pristine graphene. At the same time, the HOMO leading edge of CuPc moves toward to higher binding energy part and finally locates at ~ 1.10 eV below Fermi level (Fig. 5b). The relatively small vacuum level shift indicates that there is no significant charge transfer at CuPc/graphene interface. However, the degree of charge transfer at CuPc/O_2-G interface is much stronger than that at CuPc/graphene interface. As shown in Fig. 6a,

a much larger vacuum shift of ~ 0.82 eV to lower kinetic energy part is observed with the increasing coverage of CuPc films. Meanwhile, the HOMO leading edge of CuPc moves toward to higher binding energy part and finally locates at ~ 0.80 eV below Fermi level. More importantly, at the initial stage of the growth of CuPc (0.5 nm) on O_2-G, the HOMO leading edge of CuPc locates very close to the substrate Fermi level (Fig. 6b), indicating the Fermi level pinning behavior which facilitate the extraction of holes at CuPc/O2-G interface. As we have shown in Fig. 1a, the WF of pristine graphene increases from ~ 4.40 eV to ~ 4.92 eV after O_2 plasma treatments. As a result, the WF of O_2-G is nearly the same as or even larger than the ionization potential (IP) of CuPc films, leading to the spontaneously charge (electrons) transfer from CuPc films to O_2-G upon contact, and hence the much stronger charge transfer at the interface. The increased WF of O_2-G allows for the built-in electrical field across the active layer and for holes to transport towards the anode, resulting in the enhanced device performance for graphene-based OPVs using GO as HTL or treating graphene anode with UV/ozone.[15, 19] For the growth of CuPc films on pristine graphene, since the WF is only ~ 4.40 eV which is smaller than the IP of CuPc films, the relatively high energy barrier (the energy offset between the HOMO of CuPc and substrate Fermi level) weakens the charge transfer at the interface. Fig. S2 shows the thickness-dependent UPS spectra for the growth of CuPc on graphene sample exposed to O_2 plasma (2.0 W) for 120 s. Since the WF of the mildly O_2 plasma treated graphene (~ 4.70 eV) is also higher than the pristine graphene sample, the interfacial charge transfer is stronger than that at CuPc/graphene interface.

The schematic energy level diagrams at CuPc/graphene and CuPc/O_2-G interfaces are shown in Fig. 7a and b. It is worthy noticing that the energy offset between the HOMO of CuPc and Fermi level of O_2-G is ~ 0.80 eV, whereas it increases to ~ 1.10 eV for the growth of CuPc on pristine graphene. A smaller energy offset between the HOMO of CuPc and Fermi level of anode is beneficial to reduce the possible energy loss during the hole extraction process,[47] and hence the enhanced device performance. In addition, it can be found that the IP of CuPc is different for CuPc on pristine graphene (~ 5.20 eV) and O_2-G (~ 4.90 eV) substrate. This is attributed to the

orientation-dependent IP for organic materials.[48] According to previous studies,[49-51] CuPc molecules adopt a lying-down configuration with their molecular plane nearly parallel to the pristine graphene substrate. However, since the π-π interaction between CuPc molecules and the basal plane of graphene is disrupted in the presence of oxygenated species on O_2-G, the CuPc molecular plane becomes tilting with respect to the substrate. The different molecular orientations on pristine graphene and O_2-G substrates are responsible for the different IP of CuPc films.

Conclusions

We have demonstrated the manipulation of charge transfer at CuPc/graphene interface by treating the pristine graphene with O_2 plasma. Due to the introduction of oxygenated species on graphene basal plane, stronger degree of charge transfer is observed at CuPc/O_2-G interface compared to that at CuPc/graphene interface, which is attributed to the increased WF of graphene, or p-type doping of graphene after O_2 plasma treatments. The increased WF of O_2-G in combination with the relatively smaller energy offset between the HOMO of CuPc and Fermi level of O_2-G facilitate the extraction of holes at the interface, and hence the enhanced device performance for graphene-based OPVs.

Acknowledgements

Authors acknowledge the financial support from the National Natural Science Foundation of China (Grant No. 11104054), scientific research fund of Zhejiang provincial education department (Y201328242 and Y201430533) and HZNU research foundation for returned scholar.

REFERENCES

1. X. M. He, F. Gao, G. L. Tu, D. G. Hasko, S. Huttner, N. C. Greenham, U. Steiner, R. H. Friend and W. T. S. Huck, *Advanced Functional Materials*, 2011, 21, 139-146.
2. J. Meyer, R. Khalandovsky, P. Gorrn and A. Kahn, *Advanced Materials*, 2011, 23, 70-73.
3. G. Li, R. Zhu and Y. Yang, *Nature Photonics*, 2012, 6, 153-161.
4. Y. M. Sun, G. C. Welch, W. L. Leong, C. J. Takacs, G. C. Bazan and A. J. Heeger, *Nature Materials*, 2012, 11, 44-48.
5. Z. C. He, C. M. Zhong, S. J. Su, M. Xu, H. B. Wu and Y. Cao, *Nature Photonics*, 2012, 6, 591-595.
6. R. F. Service, *Science*, 2011, 332, 293-293.
7. M. Jorgensen, K. Norrman, S. A. Gevorgyan, T. Tromholt, B. Andreasen and F. C. Krebs, *Advanced Materials*, 2012, 24, 580-612.
8. M. C. Scharber, D. Wuhlbacher, M. Koppe, P. Denk, C. Waldauf, A. J. Heeger and C. L. Brabec, *Advanced Materials*, 2006, 18, 789-794.
9. X. Wan, G. Long, L. Huang and Y. Chen, *Advanced Materials*, 2011, 23, 5342-5358.
10. S. Pang, Y. Hernandez, X. Feng and K. Müllen, *Advanced Materials*, 2011, 23, 2779-2795.
11. H. Y. Mao, Y. H. Lu, J. D. Lin, S. Zhong, A. T. S. Wee and W. Chen, *Progress in Surface Science*, 2013, 88, 132-159.
12. Y. F. Xu, G. K. Long, L. Huang, Y. Huang, X. J. Wan, Y. F. Ma and Y. S. Chen, *Carbon*, 2010, 48, 3308-3311.
13. J. B. Wu, H. A. Becerril, Z. N. Bao, Z. F. Liu, Y. S. Chen and P. Peumans, *Applied Physics Letters*, 2008, 92, 263302.
14. Y. Wang, S. W. Tong, X. F. Xu, B. Ozyilmaz and K. P. Loh, *Advanced Materials*, 2011, 23, 1514-1518.
15. Y. Wang, X. H. Chen, Y. L. Zhong, F. R. Zhu and K. P. Loh, *Applied Physics Letters*, 2009, 95, 063302.
16. T. T. Feng, D. Xie, H. Tian, P. G. Peng, D. Zhang, D. Fu, T. L. Ren, X. M. Li, H. W. Zhu and Y. P. Jing, *Materials Letters*, 2012, 73, 187-189.
17. J. Hwang, F. Amy and A. Kahn, *Organic Electronics*, 2006, 7, 387-396.
18. F. C. Krebs, *Solar Energy Materials and Solar Cells*, 2008, 92, 685-685.
19. S.-S. Li, K.-H. Tu, C.-C. Lin, C.-W. Chen and M. Chhowalla, *ACS Nano*, 2010, 4, 3169-3174.
20. I. P. Murray, S. J. Lou, L. J. Cote, S. Loser, C. J. Kadleck, T. Xu, J. M. Szarko, B. S. Rolczynski, J. E. Johns, J. Huang, L. Yu, L. X. Chen, T. J. Marks and M. C. Hersam, *The Journal of Physical Chemistry Letters*, 2011, 2, 3006-3012.
21. Y. Gao, H.-L. Yip, S. K. Hau, K. M. O'Malley, N. C. Cho, H. Chen and A. K.-Y. Jen, *Applied Physics Letters*, 2010, 97, 203306.
22. J. Liu, Y. Xue, Y. Gao, D. Yu, M. Durstock and L. Dai, *Advanced Materials*, 2012, 24, 2228-2233.
23. J.-M. Yun, J.-S. Yeo, J. Kim, H.-G. Jeong, D.-Y. Kim, Y.-J. Noh, S.-S. Kim, B.-C. Ku and S.-I. Na, *Advanced Materials*, 2011, 23, 4923-4928.
24. X. D. Liu, H. Kim and L. J. Guo, *Organic Electronics*, 2013, 14, 591-598.
25. K. C. Kwon, W. J. Dong, G. H. Jung, J. Ham, J.-L. Lee and S. Y. Kim, *Solar Energy Materials and Solar Cells*, 2013, 109, 148-154.
26. L. M. Chen, Z. Xu, Z. R. Hong and Y. Yang, *Journal of Materials Chemistry*, 2010, 20, 2575-2598.

27. Z. Q. Xu, J. Li, J. P. Yang, P. P. Cheng, J. Zhao, S. T. Lee, Y. Q. Li and J. X. Tang, *Applied Physics Letters*, 2011, 98, 253303.
28. Q. H. Wu, Y. Q. Zhao, G. Hong, J. G. Ren, C. D. Wang, W. J. Zhang and S. T. Lee, *Carbon*, 2013, 65, 46-52.
29. S. Braun, W. R. Salaneck and M. Fahlman, *Advanced Materials*, 2009, 21, 1450-1472.
30. N. Koch, *Chemphyschem*, 2007, 8, 1438-1455.
31. H. Y. Mao, F. Bussolotti, D. C. Qi, R. Wang, S. Kera, N. Ueno, A. T. S. Wee and W. Chen, *Organic Electronics*, 2011, 12, 534-540.
32. I. Hancox, P. Sullivan, K. V. Chauhan, N. Beaumont, L. A. Rochford, R. A. Hatton and T. S. Jones, *Organic Electronics*, 2010, 11, 2019-2025.
33. N. R. Armstrong, W. N. Wang, D. M. Alloway, D. Placencia, E. Ratcliff and M. Brumbach, *Macromolecular Rapid Communications*, 2009, 30, 717-731.
34. S. W. Cho, L. F. J. Piper, A. DeMasi, A. R. H. Preston, K. E. Smith, K. V. Chauhan, P. Sullivan, R. A. Hatton and T. S. Jones, *Journal of Physical Chemistry C*, 2010, 114, 1928-1933.
35. Q. H. Wu, G. Hong and S. T. Lee, *Organic Electronics*, 2013, 14, 542-547.
36. S. Krischok, P. Stracke and V. Kempter, *Applied Physics a-Materials Science & Processing*, 2006, 82, 167-173.
37. Z. Luo, S. Lim, Z. Tian, J. Shang, L. Lai, B. MacDonald, C. Fu, Z. Shen, T. Yu and J. Lin, *Journal of Materials Chemistry*, 2011, 21, 8038-8044.
38. M. A. Pimenta, G. Dresselhaus, M. S. Dresselhaus, L. G. Cancado, A. Jorio and R. Saito, *Physical Chemistry Chemical Physics*, 2007, 9, 1276-1291.
39. A. Nourbakhsh, M. Cantoro, T. Vosch, G. Pourtois, F. Clemente, M. H. van der Veen, J. Hofkens, M. M. Heyns, S. De Gendt and B. F. Sels, *Nanotechnology*, 2010, 21, 435203.
40. A. Das, S. Pisana, B. Chakraborty, S. Piscanec, S. K. Saha, U. V. Waghmare, K. S. Novoselov, H. R. Krishnamurthy, A. K. Geim, A. C. Ferrari and A. K. Sood, *Nature Nanotechnology*, 2008, 3, 210-215.
41. J. Yan, Y. B. Zhang, P. Kim and A. Pinczuk, *Physical Review Letters*, 2007, 98, 166802.
42. L. Liu, S. M. Ryu, M. R. Tomasik, E. Stolyarova, N. Jung, M. S. Hybertsen, M. L. Steigerwald, L. E. Brus and G. W. Flynn, *Nano Letters*, 2008, 8, 1965-1970.
43. Q. Z. Hao, S. M. Morton, B. Wang, Y. H. Zhao, L. Jensen and T. J. Huang, *Applied Physics Letters*, 2013, 102, 011102.
44. S. Huh, J. Park, Y. S. Kim, K. S. Kim, B. H. Hong and J.-M. Nam, *ACS Nano*, 2011, 5, 9799-9806.
45. V. C. Tung, M. J. Allen, Y. Yang and R. B. Kaner, *Nature Nanotechnology*, 2009, 4, 25-29.
46. X. X. Yu, H. B. Cai, W. H. Zhang, X. J. Li, N. Pan, Y. Luo, X. P. Wang and J. G. Hou, *ACS Nano*, 2011, 5, 952-958.
47. H. Y. Mao, R. Wang, J. Q. Zhong, S. Zhong, J. D. Lin, X. Z. Wang, Z. K. Chen and W. Chen, *Journal of Materials Chemistry C*, 2013, 1, 1491-1499.
48. S. Duhm, G. Heimel, I. Salzmann, H. Glowatzki, R. L. Johnson, A. Vollmer, J. P. Rabe and N. Koch, *Nat Mater*, 2008, 7, 326-332.
49. I. Salzmann, A. Moser, M. Oehzelt, T. Breuer, X. Feng, Z.-Y. Juang, D. Nabok, R. G. Della Valle, S. Duhm, G. Heimel, A. Brillante, E. Venuti, I. Bilotti, C. Christodoulou, J. Frisch, P. Puschnig, C. Draxl, G. Witte, K. Müllen and N. Koch, *ACS Nano*, 2012, 6, 10874-10883.
50. H. Y. Mao, R. Wang, Y. Wang, T. Chao Niu, J. Qiang Zhong, M. Yang Huang, D. Chen Qi, K. Ping Loh, A. Thye Shen Wee and W. Chen, *Applied Physics Letters*, 2011, 99, 093301.

51. S. Zhong, J. Q. Zhong, H. Y. Mao, R. Wang, Y. Wang, D. C. Qi, K. P. Loh, A. T. S. Wee, Z. K. Chen and W. Chen, *ACS Applied Materials & Interfaces*, 2012, 4, 3134-3140.

Figure captions:

Figure 1 UPS spectra at (a) the low kinetic energy region (secondary electron cutoff) and (b) the low binding energy region (valence band region) for pristine CVD graphene and O_2-G with different exposure times.

Figure 2 (a) Raman spectra for graphene on SiO_2/Si before and after O_2 plasma treatments; (b) G and (c) 2D band Raman shifts after O_2 plasma treatments.

Figure 3 XPS spectra of (a) pristine graphene and (b-d) O_2-G for C1s core level.

Figure 4 The change of water contact angle on graphene after O_2 plasma treatments.

Figure 5 UPS spectra at (a) the low kinetic energy region (secondary electron cutoff), and (b) the low binding energy region (valence band region) during the sequential deposition of 10.0 nm CuPc on the pristine CVD graphene.

Figure 6 UPS spectra at (a) the low kinetic energy region (secondary electron cutoff), and (b) the low binding energy region (valence band region) during the sequential deposition of 10.0 nm CuPc on the O_2-G.

Figure 7 Schematic energy level diagram of CuPc on (a) pristine CVD graphene and (b) O_2-G.

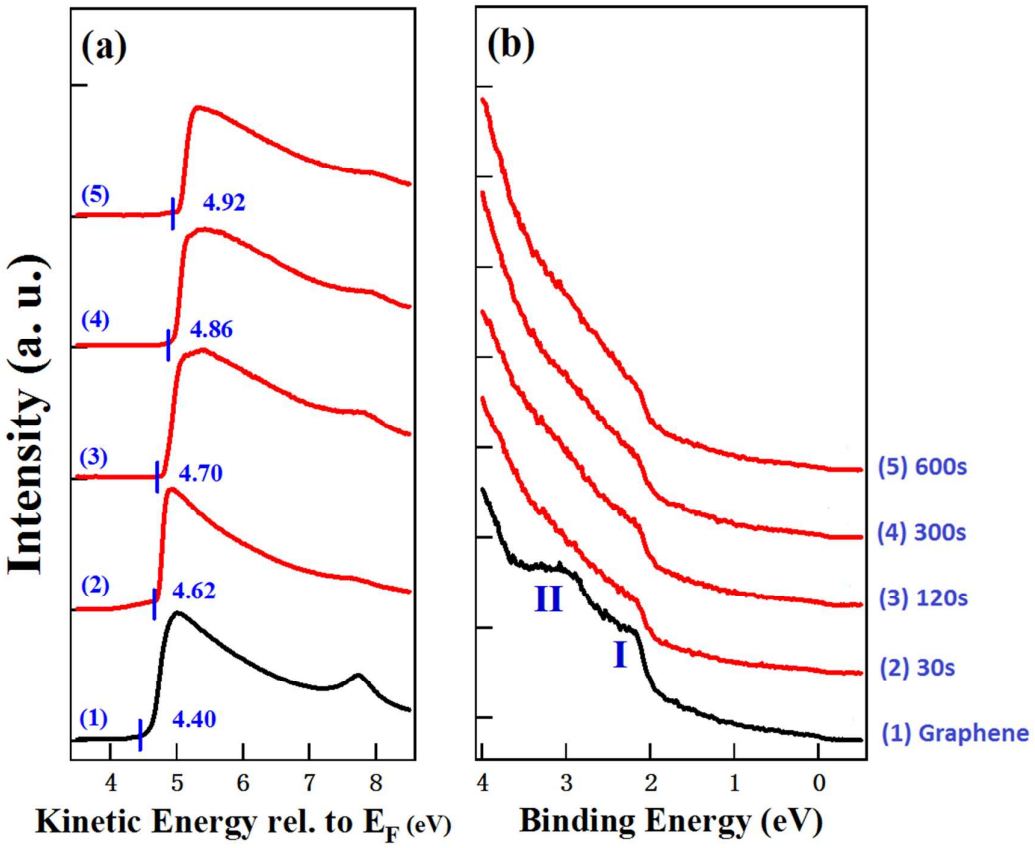

Figure 1

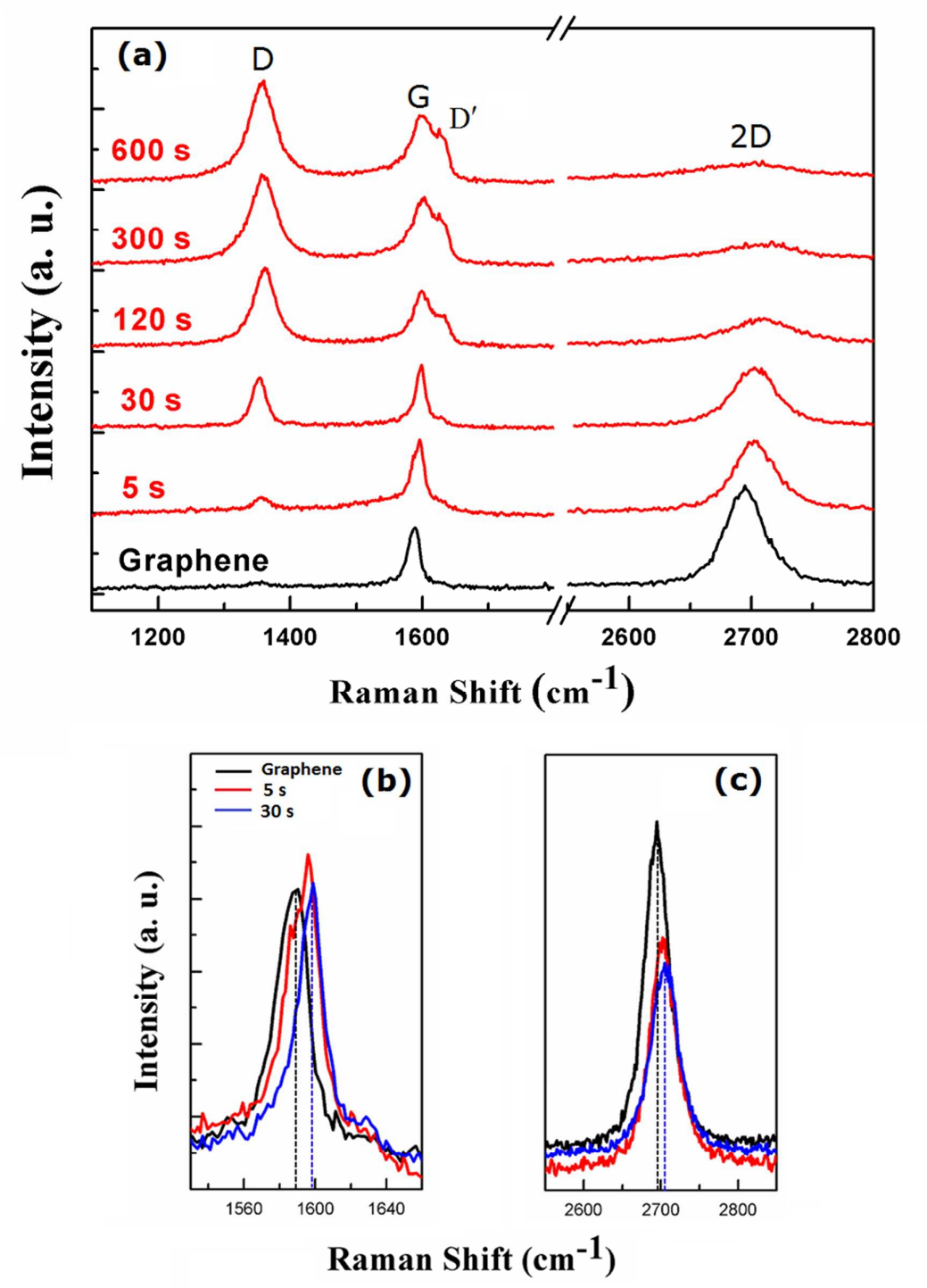

Figure 2

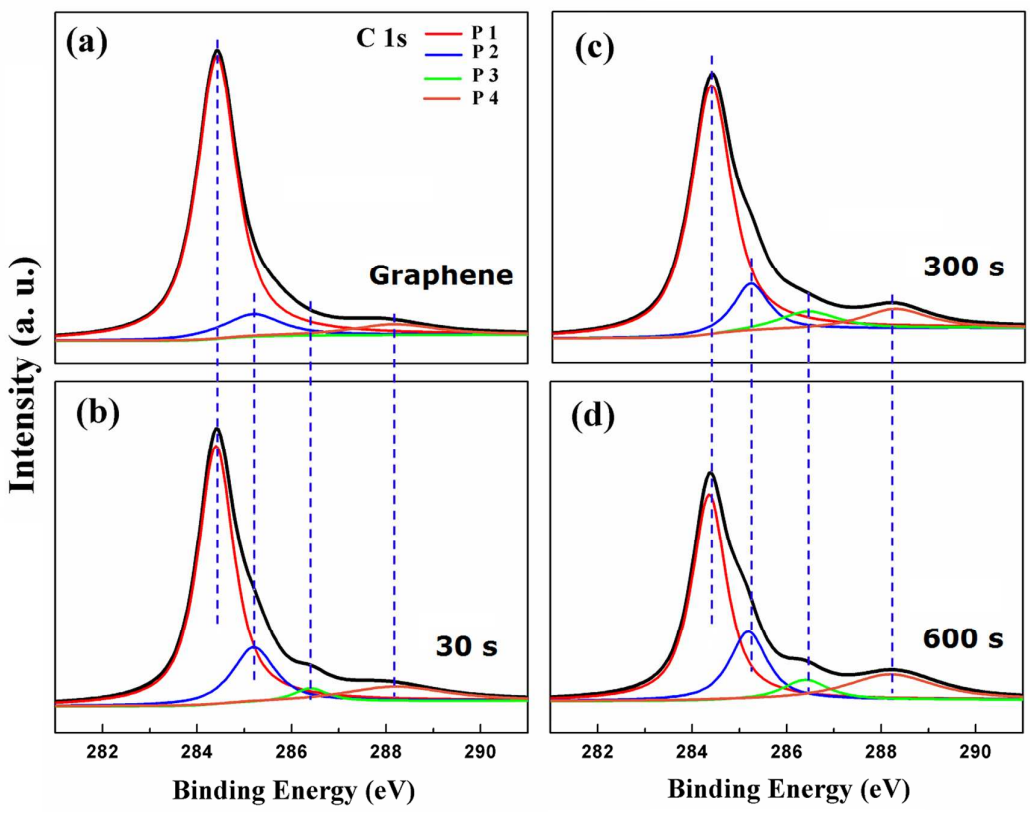

Figure 3

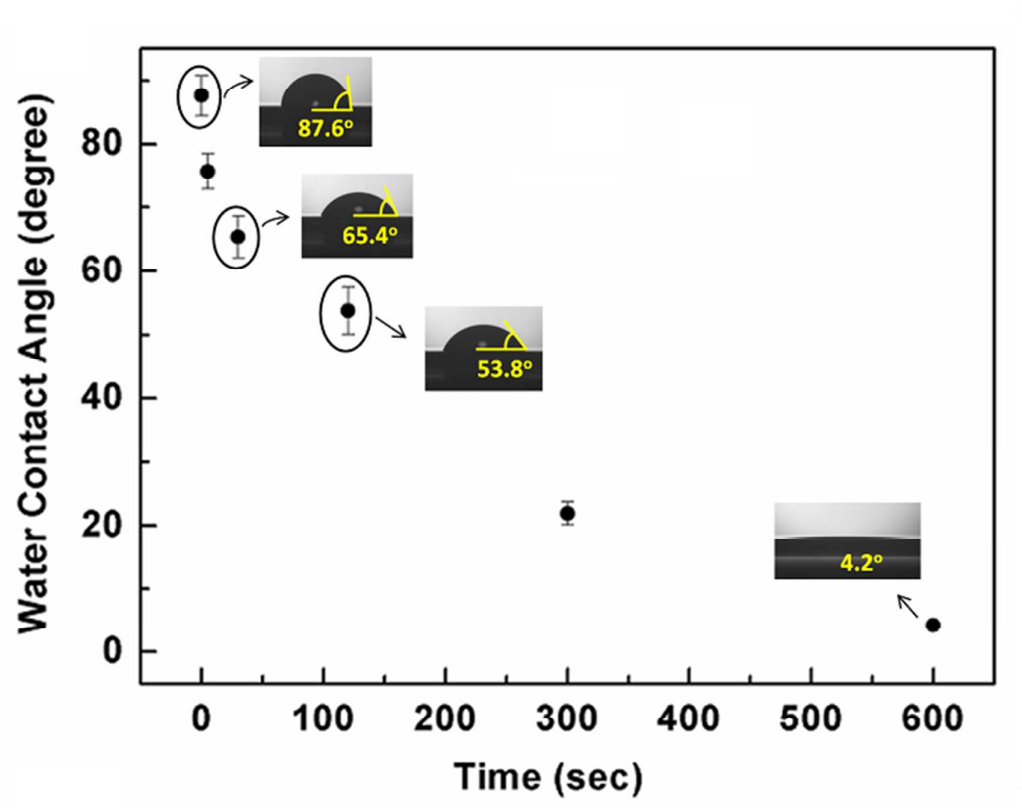

Figure 4

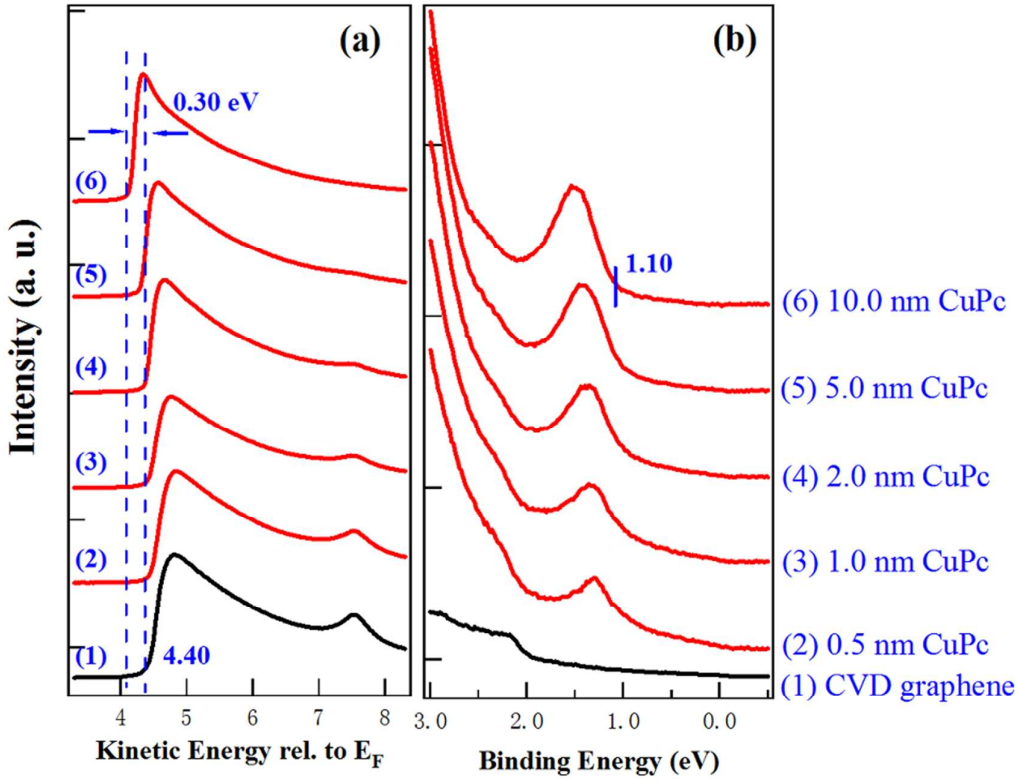

Figure 5

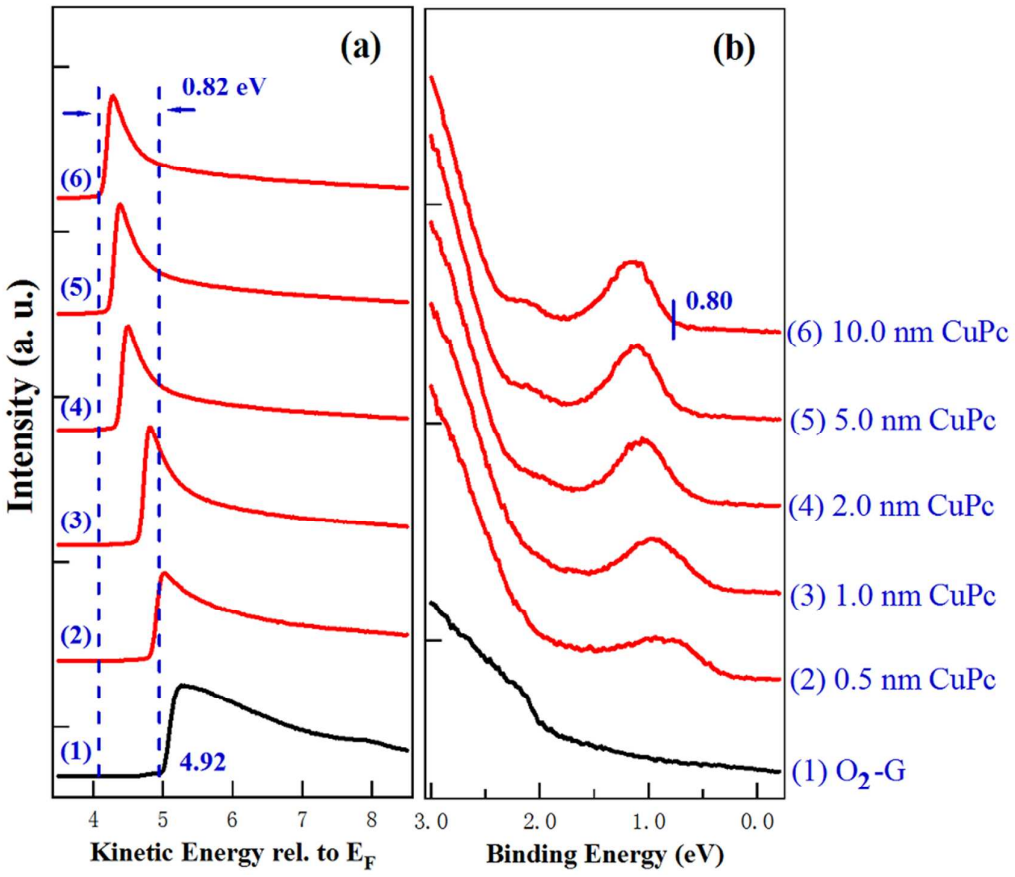

Figure 6

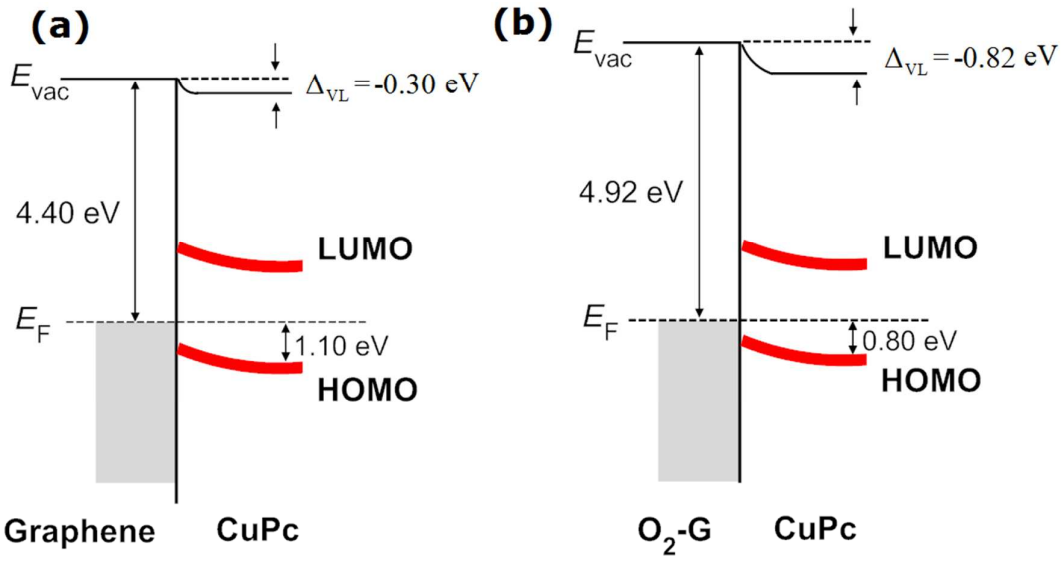

Figure 7